BIOLOGY

Dynamic Modulation of Regulatory Domain of Myosin Heads by pH, Ionic Strength and RLC Phosphorylation in Synthetic Myosin Filaments

Adhikari, B., NHMFL
Somerset, J., NHMFL
Stull, J.R., Univ. of Texas, Physiology and Southwestern Medical Center at Dallas
Fajer, P.G., NHMFL/FSU, Biological Sciences and Institute for Molecular Biophysics

The relative geometry of the myosin head with respect to the filament backbone is a function of pH, ionic strength (μ) and the extent of regulatory light chain (RLC) phosphorylation. The object of this study is to examine the dynamics of the proximal part of the myosin head (regulatory domain) that accompanies the changes in head disposition. The essential light chain was labeled at cys177 with the indane dione spin label followed by the exchange of the labeled proteins into myosin. The mobility of the labeled domain was investigated with saturation transfer electron paramagnetic resonance in reconstituted myosin filaments. We have found that the release of the heads from the myosin filament surface by reduction of electrostatic charge is accompanied by 2-fold increase in the mobility of the regulatory domain, in agreement with similar observation on the catalytic domain (Ludescher *et al*., 1988). Phosphorylation of the RLC by myosin light chain kinase resulted in a smaller 1.5-fold increase of motion establishing that the head disordering observed by electron microscopy (Levine *et al*., 1996) is due to increased mobility of the heads. This result indirectly supports the mechanism postulated by Sweeney, Bowman and Stull (1993) in which the RLC phosphorylation effect on potentiation of force arises from a release of heads from the filament surface and a shift of the heads toward actin.

Dynamics of Regulatory Light Chain of Myosin

Baumann, B., NHMFL/Biophysics Graduate Program
Hambly, B., Univ. of Sydney, Australia, Pathology
Hideg, K., Univ. of Pécs, Hungary, Institute of Organic and Medicinal Chemistry
Fajer, P.G., NHMFL/FSU, Biological Sciences and Institute for Molecular Biophysics

Motional dynamics of mutant regulatory light chain (RLC) was measured using saturation transfer EPR in synthetic myosin filaments. A mutant light chain containing a single cysteine (C154) was expressed in *E. coli* and labeled in solution with indane dione spin label. The labeled environment restricts the motional freedom of the label as visualized by molecular modeling (see Sale and Fajer report elsewhere in this volume) making it an ideal site for studying protein motion. The labeled protein was exchanged into myosin preserving its functionality as measured by ATPase activity. Effective rotational correlation times for labeled RLC were significantly shorter than those obtained for labels on neighboring essential light chain and distal motor domain; τ_ρ = 100, 20 and 7 μs respectively. These differences reflect presence of internal flexibility/hinges within myosin head. The observed flexibility might be modulated by the chemical states of ATPase cycle and provide an additional constraint of force generation models.

There an increasing body of experimental evidence that phosphorylation of the regulatory light chain is an important modulatory mechanism of myosin function e.g. in smooth muscle the phosphorylation is the activating mechanism for muscle contraction. Comparison of the RLC dynamics in the phosphorylated and dephosphorylated myosin reveals changes in rotational correlation time. Changes of motional freedom and associated steric restrictions might well provide a structural mechanism by which phosphorylation regulates ATPase activity.

EPR on Biological Samples Beyond the Limits of Superconducting Magnets—The Primary Donor Radical Cation in *Rhodobacter sphaeroides* R26 at 330 and 670 GHz

Bratt, P.J., NHMFL/UF, Chemistry
Ringus, E., Columbia College, Chemistry
Hassan, A., NHMFL
Van Tol, H., NHMFL
Rohrer, M., NHMFL
Maniero, A.L., NHMFL
Brunel, L.C., NHMFL
Bubenzer-Hange, C., Universität München, Germany
Scheer, H., Universität München, Germany
Angerhofer, A., NHMFL/UF, Chemistry

A useful approach to characterizing the electronic structure of the radical intermediates in the course of the photosynthetic charge separation is to determine the anisotropy of their *g*-matrix, which reflects the symmetrical properties of the radicals. This is especially important for the electron donor, a chlorophyll dimer species, and can not be done with conventional EPR at low field/frequency combinations. Here we report on ultra-high field EPR on the primary donor radical cation, $P_{850}^{+\cdot}$, from the purple photosynthetic bacterium *Rhodobacter sphaeroides* R26.

The X-Band EPR spectrum of chemically oxidized reaction centers (RC) of *Rb. sphaeroides* R26 at 20 K is shown in Figure 1A (experimental parameters are included in the figure caption). The linewidth is 1.14 ± 0.04 mT, which is diagnostic of the more asymmetric form of the primary donor radical cation, $P_{850}^{+\cdot}$.[1] The determination of the *g*-matrix of the primary donor radical was achieved by simulating the superimposed spectra of the radical and the Mn^{2+} *g*-standard (see Figure 1B), with an absolute error of $\delta g = \pm 5 \times 10^{-5}$.[2] The simulation gave the following *g*-values: $g_{xx} = 2.00323$, $g_{yy} = 2.00241$, and $g_{zz} = 2.00197$. Unlike $P_{700}^{+\cdot}$,[2] the *g*-values do not appear to be temperature dependent, and the spectra at higher temperatures could also be fitted using the same set of values (see Figure 2).

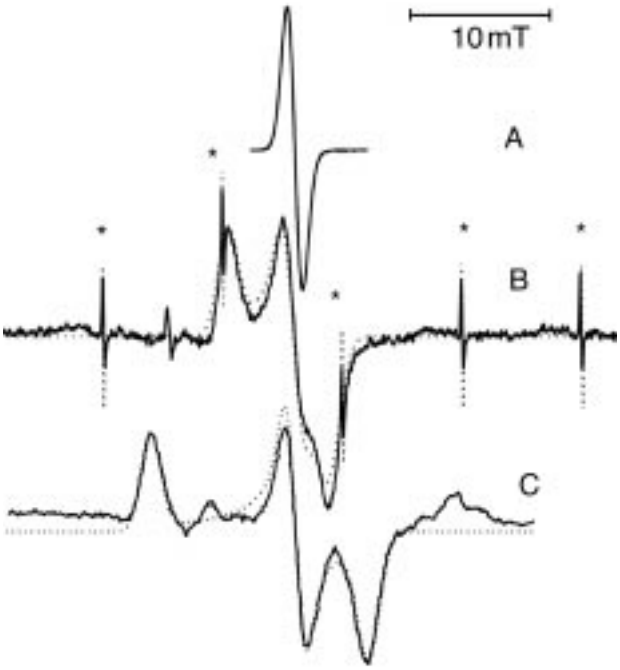

Figure 1. EPR spectra of the primary donor radical cation in *Rb. sphaeroides* R26 RCs at different magnetic field strengths at 10 K. (A) 9.43785 GHz, center field is at 0.33677 T. (B) 327.690 GHz, solid line is the experimental spectrum, dashed line is the simulation. The sharp lines marked with asterisks arise from the MnO standard used as a field calibration as described in the text. The center field is at 11.68015 T. (C) 670.463 GHz, solid line is the experimental spectrum, and dashed line is the simulation. The center field is at 23.92745 T.

Higher fields were available for EPR with the new Keck magnet (up to 25 T with high homogeneity), which was used for the following purposes:

a. To obtain better spectral resolution and fully resolve the g_{yy} and g_{zz} components.
b. To test the primary donor radical cation for possible *g*-strain (*g*-factor heterogeneity).
c. To demonstrate the feasibility of high field EPR experiments on biological samples using fields above 20 T.

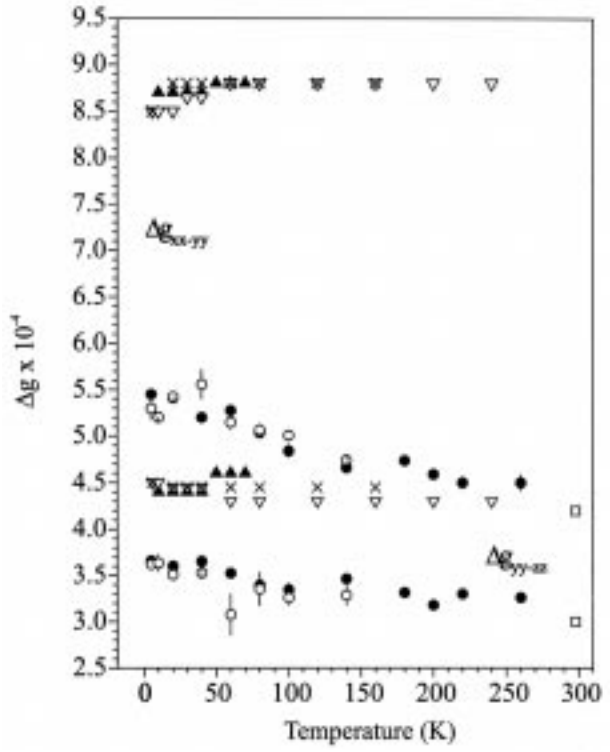

Figure 2. Temperature dependence of the $P^{+\cdot}_{865}$ D*g*'s as a function of temperature, compared with similar data from $P^{+\cdot}_{700}$.[2] For $P^{+\cdot}_{700}$ the filled circles (•) indicate that the measurements were made using Triton X-100 preparations of PS I RCs, and the open circles (o) indicate a digitonin preparation. The *g*-values obtained by Prisner, *et al*.,[3] are shown as open squares (❑) for comparison at 296 K. The D*g*-values obtained for $P^{+\cdot}_{850}$ in LDAO without glycerol are shown as open triangles pointing down (∇) for the data obtained at 330 GHz, and as filled triangles pointing up (▲) for the data at 670 GHz. Data for the RCs in LDAO with glycerol at 330 GHz are presented with crosses (x).

We were able to obtain excellent resolution at 670 GHz, (23.9 T), where g_{yy} and g_{zz} are completely resolved. The spectrum taken at 670 GHz is shown in Figure 1C.

From both data sets, it is clear that the *g*-values of the bacterial primary donor radical do not change appreciably with temperature (see Figure 2). This is in marked contrast with the primary donor of PS I, $P^{+\cdot}_{700}$, where the spectrum becomes more isotropic with increasing temperature.[2]

The apparent insensitivity of the *g*-values, to temperature in RCs of *Rb. Sphaeroides*, indicates that the distribution of the wavefunction over the special pair of bacteriochlorophyll molecules does not change with temperature.

One of the most striking findings of our experiments is that there is negligible *g*-strain in the primary donor radical cation. The linewidths used for successful simulations of the high field spectra were between 1.1 mT and 1.4 mT (lines broadened at lower temperatures), and did not have to be increased for the simulations of the spectra taken at 670 GHz. This signals a remarkable homogeneity of the primary donor in our sample quite unlike the spectra of oxidized monomeric chlorophyll species in frozen organic solvents, where *g*-strain dominates the linewidth above 300 GHz.

References:

1 Müh, F., *et al*., Biochemistry, 36, 4155-4162 (1997).
2 Bratt, P.J., *et al.*, J. Phys. Chem. B, 101, 9686-9689 (1997).
3 Prisner, T.F., *et al*., Proc. Natl. Acad. Sci. USA, 90, 9485-9488 (1993).

High Field EPR on the Deuterated Chlorophyll *a* Radical Cation

Bratt, P.J., NHMFL/UF, Chemistry
Krzystek, J., NHMFL
Brunel, L.C., NHMFL
Polouektov, O., Argonne National Laboratory
Thurnauer, M., Argonne National Laboratory
Angerhofer, A., NHMFL/UF, Chemistry

High field EPR at field/frequency combinations of 11 T/300 GHz, and above, has been successfully used in the past to unravel the *g*-factor anisotropy of the primary donor radical cation of plant photosystem I (PS I).[1] Here we report on similar results on deuterated Chlorophyll *a* (Chl) radical cations in an organic solvent glass. The present data are needed for the interpretation of the *in vivo* spectra, and provide the frame in which *g*-factor shifts need to be interpreted.

Preliminary experiments with protonated Chl *a* showed that there was insufficient resolution at fields as high as 24 T (data not shown). Figure 1 shows a continuous wave (cw) EPR experiment performed on fully deuterated Chl *a* at 330 GHz together with a simulation providing the following principal values of the anisotropic *g*-matrix: $g_{xx} = 2.00330 \pm 10^{-5}$, $g_{yy} = 2.00277 \pm 10^{-5}$, and $g_{zz} = 2.00230 \pm 10^{-5}$. These values are slightly more anisotropic than those of PS I ($g_{xx} = 2.00317 \pm 10^{-5}$, $g_{yy} = 2.00264 \pm 10^{-5}$, and $g_{zz} = 2.00226 \pm 10^{-5}$),[1] which demonstrates the effect of dimerization in PS I on the electronic structure of the radical cations. From ENDOR data it is concluded that the primary donor radical cation in PS I is an asymmetric dimer with a 3:1 electron density distribution over the special Chl pair.[2] This partial delocalization is responsible for the more isotropic *g*-matrix in PS I.

Quantitation of the effect at this stage has to await a quantum-theoretical study of the *g*-anisotropy in Chl. A first estimate of the temperature dependence of the delocalization of the electronic wavefunction in PS I, however, can be performed with the present data. Under the assumption that the difference (Δg) between $g_{||} = g_{zz}$ and $g_{\perp} = (g_{xx}+g_{yy})/2$ is most sensitive to the electronic delocalization (g_{xx}-g_{yy} depends more strongly on the orientation of the two Chl molecules relative to each other, which is not known precisely for PS I), one can draw up a linear calibration scale that relates the degree of delocalization to the value of Δg, and estimate the degree of delocalization of PS I at physiological temperatures. Based on this reasoning $\Delta g \approx 7.4 \times 10^{-4}$ would be representative of a completely localized monomeric *g*-anisotropy, while $\Delta g \approx 6.5 \times 10^{-4}$ would represent a 25% admixture of the second Chl wavefunction to the total (3:1 asymmetry). Linear extrapolation, which at this point is a zero-order guess, to the fully symmetric case (50% admixture of the second Chl) would then predict a $\Delta g \approx 5.6 \times 10^{-4}$. This is approximately the anisotropy observed for PS I at temperatures above 200 K, which is suggestive of a fully symmetric dimer under physiological conditions.

The linewidths used in the simulation of the spectrum in Figure 1 were 11 G (g_{xx}), 8 G (g_{yy}), and 18 G (g_{zz}), which was more than expected for deuterated Chl. This indicates the presence of *g*-strain in the solvent glass which was confirmed with EPR at 670 GHz (data not shown) where the resolution actually became worse than at 330 GHz.

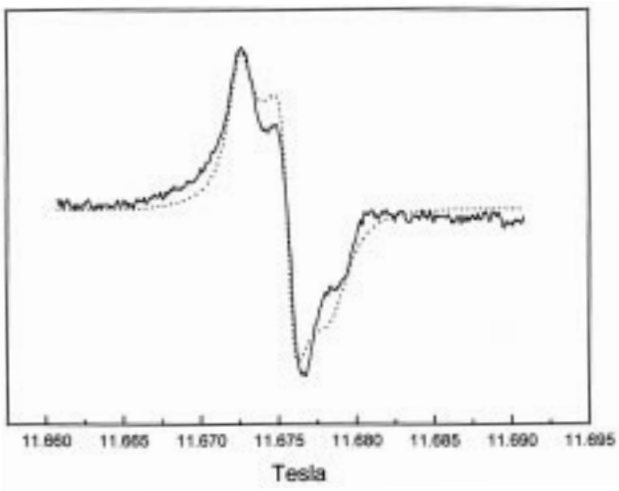

Figure 1. cw-EPR spectrum of deuterated Chl *a* radical cations in methylene chloride at 60 K (solid line) with powder spectrum simulation (broken line, values given in text).

References:

1 Bratt, P.J., *et al.*, J. Phys. Chem. B, 101, 9686-9689 (1997).

2 Käss, H.E, *et al.*, Chem. Phys., 194, 419-432 (1995).

High Field EPR Spectroscopy of the Cation Radical Primary Electron Donors of *Chlorobium limicola* and *Heliobacillus mobilus*

Bratt, P.J., NHMFL/UF, Chemistry
Heathcote, P., Univ. of London, Biology
Angerhofer, A., NHMFL/UF, Chemistry
Hassan, A., NHMFL
Maniero, A.L., NHMFL
Brunel, L.C., NHMFL

The photosynthetic reaction center of the purple non-sulfur bacterium *Rhodobacter sphaeroides* is a protein heterodimer of two core protein

subunits, designated L and M, that resemble each other, employing a bacteriochlorophyll (BChl) *a* pair as the primary electron donor. The BChl *a* pair is bound with an apparent C_2 symmetry axis of the reaction center with each BChl *a* attached to one peptide of the heterodimer. Spectroscopic analysis using ENDOR and ESEEM has shown that the unpaired electron spin in the oxidized BChl *a* pair, $P870^{\bullet+}$ is asymmetrically distributed (in a 2:1 ratio) between the constituent BChl *a* molecules.[1] This asymmetry is attributed to the influence of the two different protein subunits in the heterodimer, which are producing an asymmetry in the arrangement and energy of the prosthetic groups, which leads to efficient unidirectional electron transfer.

A heterodimer structure and asymmetric electron spin density distribution are also found in the reaction centers of oxygenic photosynthesis, where the electron distribution ratio is even more asymmetric, (3:1 in the case of $P700^{\bullet+}$ and $P680^{\bullet+}$ the primary donors of PSI and PSII). A fourth type of photosynthetic reaction center is that of green sulfur bacteria, the Chlorobiaceae and the Heliobacteriaceae. These are ferredoxin-reducing reaction centers, and are homologous in redox carrier composition and function to the photosystem I (PSI) reaction center. Despite the similarities between PS1 and the *Chlorobium limicola* reaction center, genetic analysis of *C. limicola* has found only one gene that shows homology with the large core reaction center proteins of PSI. A similar result was obtained from *Heliobacillus mobilus.* This implies that these two organisms had reaction centers that are protein homodimers. ENDOR and ESEEM studies on *Chlorobium limicola* have shown that the electron distribution is essentially 1:1.[2,3]

In order to gain further insight into the local structure surrounding the primary donor cation, we have attempted very high field EPR spectroscopy on these reaction centers using 11.6 T and 23.9 T fields. In Figures 1 and 2, the 330 GHz EPR spectra of *Chlorobium* and *Heliobacter* at 5 K are presented. Although the analysis of these two spectra is not yet completed, it may be seen that the spectra are only partially resolved even at these very high operating frequencies. Because the spectrum appeared only partially resolved at 330 GHz, we used the Keck magnet operating at 23.9 T to gain further insight into the spectrum. The spectrum that we obtained at 10 K and 670.463 GHz is shown in Figure 3. This spectrum shows considerably more resolution. Unfortunately the admixture of dispersion makes it difficult to interpret. Nevertheless, the g_{xx} component can clearly be discerned at 23.9263 T, while the g_{yy} and g_{zz} components still overlap (23.9355 T). A simulation of the spectrum was not attempted due to the distortions from dispersion admixture. The excellent separation of the g_{xx} and g_{yy} components and their relatively narrow linewidths, however, indicate high homogeneity (little or no g-strain), and would make this preparation a good candidate for high-resolution EPR beyond 1 THz.

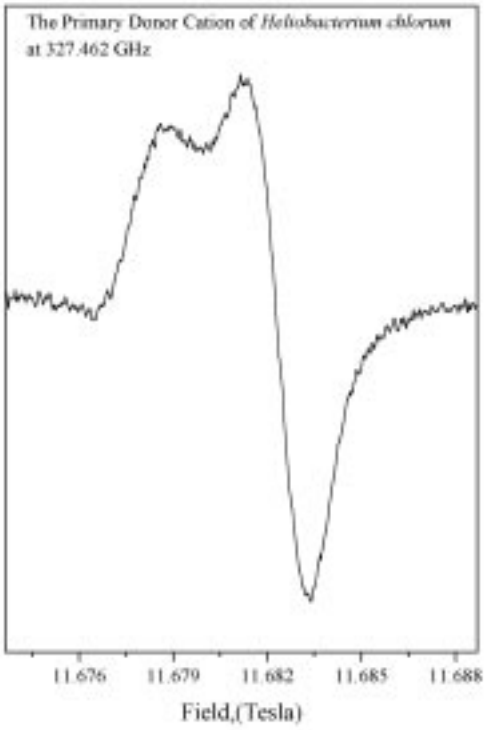

Figure 1: High field EPR spectrum of the primary donor of *Heliobacillus mobilus* at 327.462 GHz and 10 K.

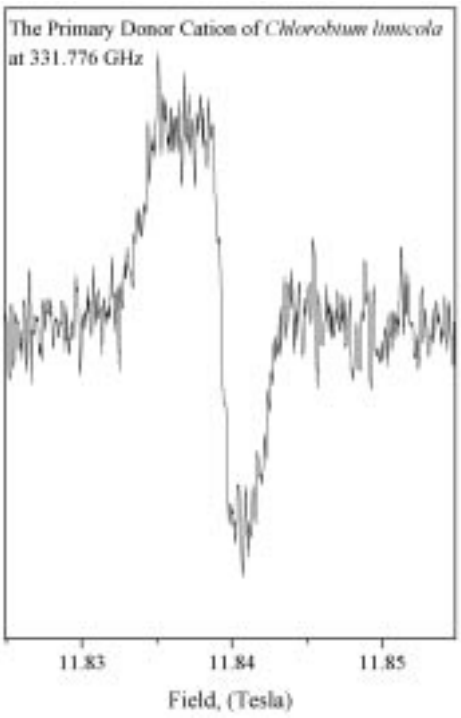

Figure 2: High field EPR spectrum of the primary donor of *Chlorobium limicola* at 331.776 GHz and 10 K.

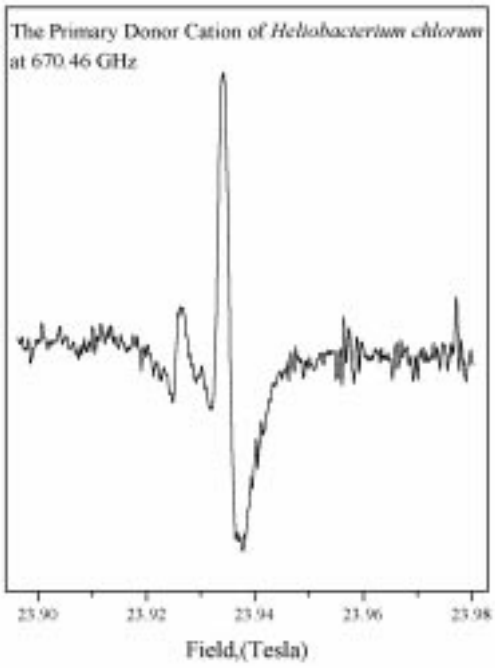

Figure 3: High field EPR spectrum of the primary donor of *Heliobacillus mobilus* at 670.46 GHz and 10 K.

References:

1 Feher, G., J. Chem. Soc., Perkin Trans., 2, 1861-1874 (1992).

2 Rigby, *et al*., Febs. Lett., 350, 24-28 (1994).

3 Bratt, P.J., *et al*., Photochemistry and Photobiology, 64(1), 20-25 (1996).

High Field EPR Studies of the Secondary Acceptors in Photosystem II, Q_A and Q_B

Bratt, P.J., NHMFL/UF, Chemistry
Smith, P.J., Univ. College London. Biology
Nugent, J.H.A., Univ. College London, Biology
Angerhofer, A., NHMFL/UF, Chemistry
Brunel, L.C., NHMFL
Krzystek, J., NHMFL
Hassan, A., NHMFL

The major impetus to understand the structure and function of Photosystem II, (PSII) is the quest to elucidate the mechanism of water oxidation, which has led to a variety of preparations of greater stability, purity and activity.[1] The reaction center of PSII is located in a dimer of proteins termed D1 and D2, which show considerable homology to the L and M polypeptides that form the reaction center of purple bacteria. Electron transfer follows the absorption of light by the primary donor chlorophyll P680. Pheophytin (Phe) acts as an intermediate electron acceptor, and two molecules of plastoquinone, Q_A and Q_B act as additional electron acceptors. The oxidizing equivalents generated by photooxidation of P680 are not reduced by cytochrome as in the purple bacteria, but by electrons from water. Oxidizing equivalents are accumulated by the Oxygen Evolving Complex (OEC), where water is oxidized to molecular oxygen.

Q_A is reduced by Phe^- 200-400 ps after P680 oxidation. Under normal conditions Q_A transfers the electron to the secondary quinone (Q_B), which is a two electron carrier. In the doubly reduced protonated from Q_BH_2, the plastoquinol dissociates from PSII, and is replaced by a plastoquinone molecule. Q_A and Q_B are both plastoquinones, so the differences in their behavior can only be a product of their protein environments. In purple bacteria, the Q_B semiquinone is stabilized in the binding site by protonation of the reaction center. Reduction of Q_B^- is believed to be coupled to protonation of

the doubly reduced quinone. In purple bacteria, the protons arrive in the binding site through a chain of protonable side chains. In PSII, a similar proton transfer system may exist, although, other mechanisms involving bicarbonate have been proposed as well. The Q_B binding site is known to be the site of action for many herbicides that act by blocking electron transfer beyond Q_A. The herbicides are thought to act by competing with Q_B, Q_B^- or Q_BH_2 for the binding pocket.

Both the Q_A and Q_B semiquinones have characteristic EPR signals, which are stable at cryogenic temperatures, and are amenable to study. In the case of $Q_A^{\bullet -}$, the most typical preparation involves TRIS washing of the material to remove extraneous manganese. It has been assumed that TRIS washing has no effect on the local structure of the semiquinone, and at X-Band the spectra of TRIS washed and native protein $Q_A^{\bullet -}$ are the same. However, we have studied the spectra of $Q_A^{\bullet -}$ in native and TRIS washed preparations at 11.6 T, and observed differences in the spectra. This is shown in Figures 1 and 2. In the case of the native protein, the g_{xx} peak is split into two peaks, which may indicate that there are two spectra superimposed differing only in the g_{xx} value. This could be a result of hydrogen bonding of one species while the other may be hydrogen bonded to a lesser extent. In the TRIS washed preparation, the two peaks have merged. The calculated values of the principal components of the g tensor are shown in the figure inset. This difference may indicate a disruption in the local order surrounding Q_A after TRIS washing. We have also measured the spectra of $Q_B^{\bullet -}$, which is shown in Figure 3, and the initial results seem to indicate that there is little difference in the anisotropic g-matrix to that of $Q_A^{\bullet -}$.

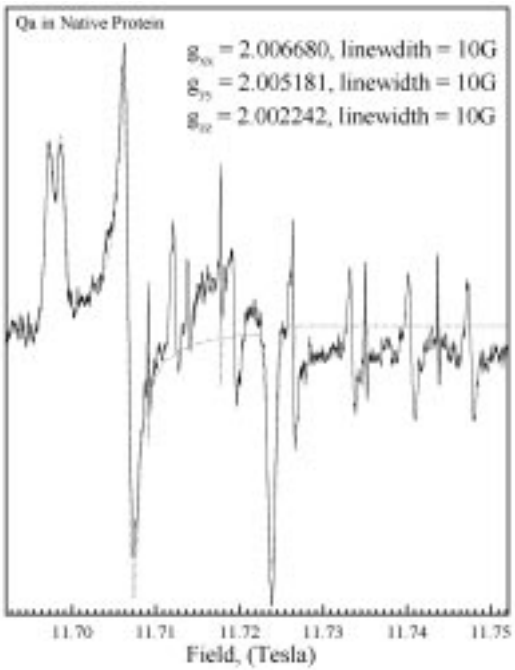

Figure 1. The EPR spectrum of Native $Q_A^{\bullet -}$ obtained at 328.548 GHz and 5 K. The sharp lines are from the Mn^{2+} standard used for calibrating the magnetic field.

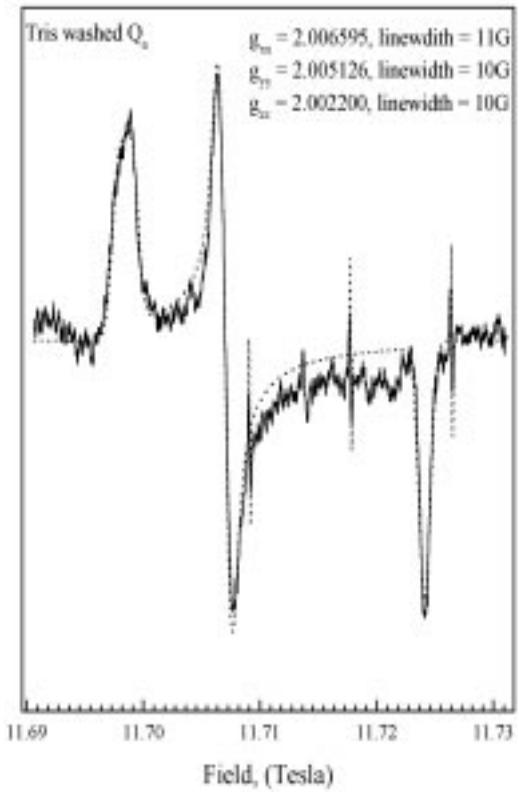

Figure 2. The EPR spectrum of TRIS washed $Q_A^{\bullet -}$ obtained at 328.548 GHz and 5 K.

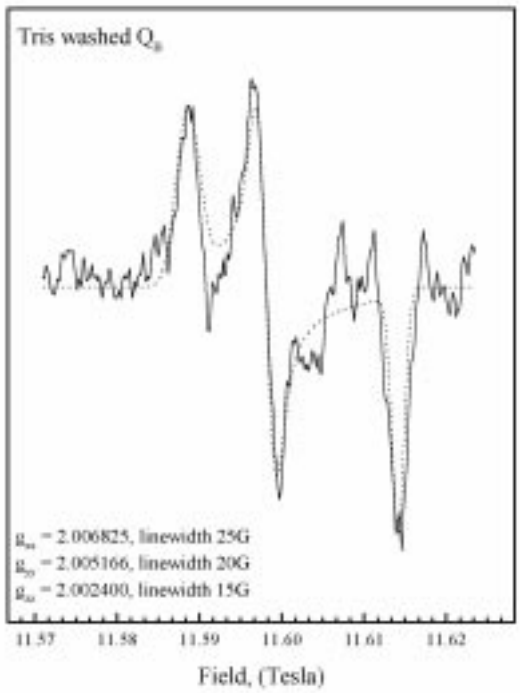

Figure 3. The EPR spectrum of TRIS washed $Q_B^{\bullet-}$ obtained at 325.497 GHz and 5 K.

Reference:

1 Evans, M.C.W., *et al*., The Photosynthetic Reaction Center, 1, 391-415 (1993).

The Primary Electron Donor Radical Cation from *Rhodopseudomonas viridis* Observed with EPR at 330 and 670 GHz

Bratt, P.J., NHMFL/UF, Chemistry
Hassan, A., NHMFL
Van Tol, H., NHMFL
Brunel, L.C., NHMFL
Heathcote, P., Queen Mary & Westfield College, Univ. of London, Biological Sciences
Angerhofer, A., NHMFL/UF, Chemistry

The primary donor radical cation of the purple photosynthetic bacterium *Rhodopseudomonas (Rps.) viridis* has been observed with cw-EPR at 330 and 670 GHz. The *g*-anisotropy could be fully resolved at the higher frequency, and partially at the lower frequency. Figure 1 shows a typical spectrum taken at 670 GHz and 23.9 T.

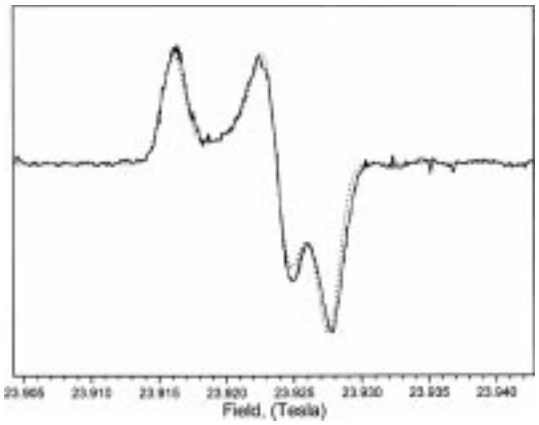

Figure 1. cw-EPR spectrum of the primary donor radical cation of chemically oxidized reaction centers from *Rhodopseudomonas viridis* at 670 GHz (solid line), and powder spectrum simulation (dotted line).

The remarkable resolution was possible because of complete lack of *g*-strain, which had also previously been observed in reaction centers (RC) from *Rhodobacter (Rb.) sphaeroides* and plant photosystem I (PS I).[1] These experiments are impossible at lower field/frequency combinations and demonstrate the necessity of fields above 20 T for high resolution EPR experiments on biological radicals.

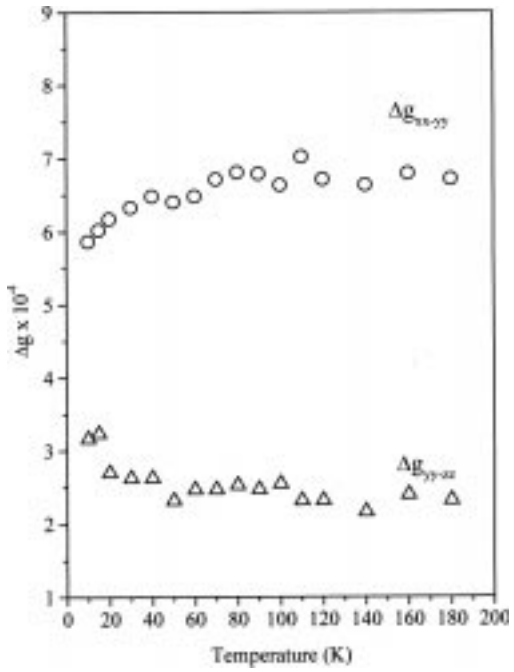

Figure 2. Temperature dependence of the differences between the principal *g*-matrix components for *Rhodopseudomonas viridis*.

The experiments described here allowed to determine the temperature dependence of the *g*-anisotropy in the range between 5 K and 180 K (see Figure 2). Contrary to the case of PS I, but similar to that of *Rb. sphaeroides*, the axial anisotropy ($g_{||} - g_{\perp}$) did not change significantly with temperature, while the rhombicity ($|g_{xx}-g_{yy}|$) increased with increasing temperature between 5 K and 70 K. This seems to indicate that the dimer character of the primary donor radical cation in the bacterial RCs does not change substantially with temperature. On the other hand there may very well be a temperature-dependent structural rearrangement of the dimer halves, possibly a rotation of the molecular planes about their (almost parallel) z-axes.

Reference:

1 Bratt, P.J., *et al*., J. Phys. Chem. B, 101, 9686-9689 (1997).

Chlorosomes Structure Investigated by High Field EPR

Carbonera, D., Univ. of Padua-Italy, Physical Chemistry
Giacometti, G., Univ. of Padua-Italy, Physical Chemistry
Vannini, C., Univ. of Milano-Italy, Structural and Functional Biology
Gerola, D., Univ. of Milano-Italy, Structural and Functional Biology
Vianelli, A., Univ. of Milano-Italy, Structural and Functional Biology
Maniero, A.L., NHMFL
Brunel, L.C., NHMFL

Light-harvesting complexes (Antenna) capture photons and transfer energy to Reaction Centers in the primary processes of natural photosynthesis. Different strategies concerning structure of antenna complexes and pigment composition have been adopted by different organisms. Chlorosomes are the antenna complexes found in green sulfur bacteria. They are anomalous since the protein content of these organelles is quite low compared to other systems and the absorption properties seem to be determined mainly by pigment-pigment interactions instead of by pigment-protein interactions.

Some hypotheses concerning the structure of chlorosomes have been formulated based on CD and optical spectroscopy as well as on NMR. Several studies on BChl *c* self-assembled oligomers "in vitro" have also been reported. The number of pigments, however, involved in the formation of oligomers and the supramolecular structure, involving different oligomers, is still a matter of debate and of investigation.

Oxidation of chlorosomes by chemicals such as potassium ferricyanide produces the formation of stable BChl *c* cations, which may be used as a probe of the structure by using EPR spectroscopy. X-band experiments have been performed in isolate chlorosomes from Chlorobium tepidum showing the presence of radical Bchl *c*. The linewidth of the EPR signal decreases from 0.9 mT to 0.3 mT as the temperature is increased form 4 K to 225 K. This effect is likely due to thermally activated electron transfer among several BChl *c* molecules in the structure. Multifrequency EPR at higher fields has been done at 110 GHz, 220 GHz, and 330 GHz. Only at the highest frequency used the g-tensor anisotropy can be partially resolved, the linewidth of the EPR signal increasing from 1.7 mT to 6.0 mT going from 110 GHz to 330 GHz (see Figure 1).

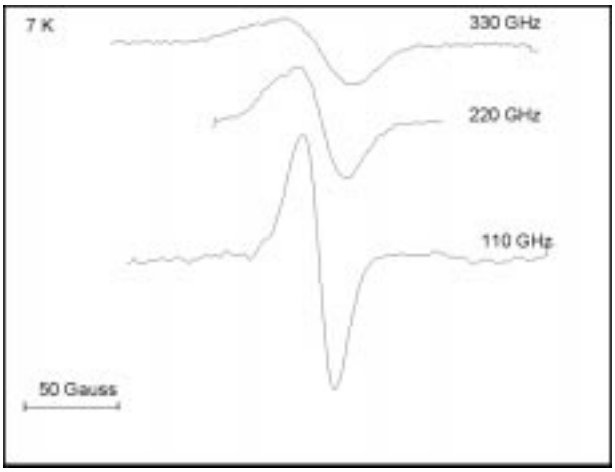

Figure 1. EPR spectra, at different frequencies, of chemically oxidized chlorosomes from *Chlorobium tepidium*.

Surprisingly the linewidth of the high field EPR signals at about 300 GHz does not change by increasing the temperature in the range from 7 K to 85 K, at higher temperature the intensity of the signals being too low to allow the detection. The same behavior is found at 110 GHz up to 160 K.

Exposure of the samples to different concentrations of potassium ferricyanide (from 1 mM to 100 mM) does not produce significant differences in the shape of the signals but only in the intensity.

Hopping of the positive hole (Electron transfer processes) between different BChl *c* molecules and/or delocalization of the charge among molecules forming oligomers are expected to take place in these antenna systems on the basis of the structural hypotheses. All these processes are, in principle, temperature dependent, and depend also on the interactions among pigments as well as on different site energies. The absence of line narrowing at high field may be due to the g–anisotropy, which becomes the most important factor on the line broadening of the signals at the higher magnetic fields.

The absence of temperature dependence of the g-tensor main values could indicate either a parallel or antiparallel arrangement of the BChl *c* planes making up the oligomers in the chlorosomes. Alternatively the electron transfer rates, in the temperature range investigated, could be to slow to mediate the g-values of the different molecules. Further investigation at higher temperatures is necessary to clear up this point.

Human Hemoglobin in High Magnetic Field

Chen, C.-J., FAMU-FSU College of Engineering
Haik, Y., FAMU-FSU College of Engineering
Pai, V.N., FAMU-FSU College of Engineering
Da Motta, M., UFPE, Recife, Brazil, Biophysics

The effects of high magnetic field on human normal and sickle hemoglobin were investigated using the facilities at the NHMFL in Tallahassee. The experiments were aimed at better understanding the behavior of human blood under high field. A review of the experiments follows.

Deoxygenated and Oxygenated Normal Hemoglobin. The effects of high static magnetic field on human deoxyhemoglobin and oxyhemoglobin spectrophotometric characteristics is studied. Five samples of partially deoxygenated hemoglobin in aqueous solution were tested. Magnetic field was applied in steps of 2 T, from 0 T to 18 T. Spectral analysis showed a higher light absorption at wavelengths of 546 nm and at 581 nm. The applied magnetic field did not alter the wavelengths at which the absorption peaks occurred. On the other hand, the light absorption was found to increase with the applied magnetic field strength up to 14 T.

Deoxygenated Sickle Hemoglobin. Sickle deoxygenated hemoglobin was obtained by bubbling nitrogen and carbon dioxide in the samples. The oxygen concentration in the sickle hemoglobin was 1.1%. High static magnetic field was applied in steps of 0.5 T, from 0 T to 6 T. Spectral analysis showed that sickle hemoglobin light absorption decreases when it is subjected to magnetic field. The absorption peak is maintained at 578 nm for the sickle hemoglobin. The absorption peak shift of sickle hemoglobin when subjected to magnetic field can be used for diagnostic purposes.

Near Infra Red (NIR) Hemoglobin Spectroscopy. Hemoglobin with high (19.5%) and low (1.3%) oxygen concentration of normal adult hemoglobin (HbA) solutions were exposed to magnetic fields ranging from 0.5 T to 6 T, in steps of 0.5 T. Light absorption of near infra red wavelengths was measured before and during the magnetic exposure. The wavelength ranged from 800 to 1100 nm. The results showed that high oxygen hemoglobin spectra have a lower absorbance as compared with the low oxygen hemoglobin spectra. The deoxygenated hemoglobin showed clustering of the spectra curves with a peak at 932 nm when the magnetic field is applied while the oxygenated hemoglobin has a distinguished spread of the absorption spectra that is increasing with the

magnetic field. The high magnetic field will affect the NIRS-based and infrared oxymetry measurements. Figures 1 and 2 show the results of high and low oxygen concentration NIR spectrums, respectively.

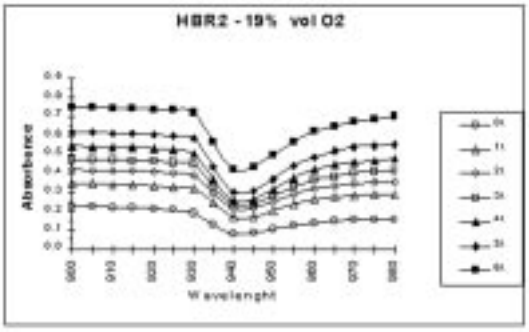

Figure 1. High oxygen concentration.

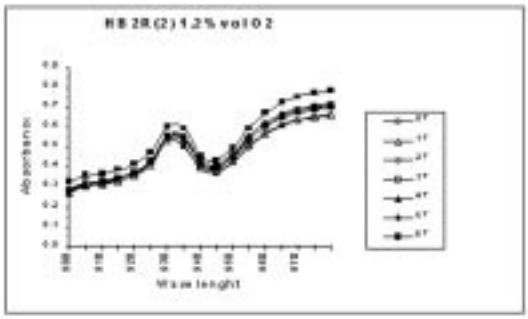

Figure 2. Low oxygen concentration.

Reference:

1 Motta, M.A., *et al*., J. Bioelectrochem & Bioenerg 97 (1998).

A PCR-Based Method for Uniform $^{13}C/^{15}N$ Labeling of Long DNA Oligomers

Chen, X., LANL
Mariappan, S.V.S., LANL
Kelly, J.J., LANL
Bushweller, J.H., LANL
Bradbury, E.M., LANL
Gupta, G., LANL

We developed a PCR-based method for uniform $^{13}C/^{15}N$ labeling of long DNA oligomers, and was used to synthesize a DNA duplex predicted to involve in the yeast replication initiation. The availability of uniformly $^{13}C/^{15}N$ labeled DNA for structure determination will enable us to enrich the distance constraint set through the many recently developed multinuclear and multidimensional NMR methods. It also will allow us to perform NOE-independent sequential assignments which are very difficult by conventional ^{1}H NMR methodology. In our attempts to understand the utility of $^{13}C/^{15}N$ labeling in the process of resonance assignment and structure determination, a series of two-dimensional homo- and hetero-nulear (^{15}N -edited and ^{13}C -edited) experiments were performed to assign the imino and amino nitrogens and their corresponding exchangeable imino and amino protons. The ^{13}C -edited experiments were performed to identify ^{13}Cs attached to the base protons (H8/H6/H5/H2). In order to circumvent the problem of low DNA concentration and poor signal-to-noise ratio, ^{13}C-^{1}H hetero-nuclear experiments were recorded on the 720 MHz spectrometer at NHMFL, Tallahassee. The data collected from the NHMFL facility provided with an important piece of result (correlating H8/H6/H5/H2 with the corresponding ^{13}Cs) strengthening the outcome of the project. We recently published the results of this project in a peer-reviewed journal (FEBS Letters, 436, 372-376 (1998)).

Structure-Function Studies of Neuropeptides

Edison, A.S., NHMFL/Univ. of Florida Brain Institute, UF Center for Structural Biology, and UF, Biochemistry & Molecular Biology
Zachariah, C., NHMFL

We have continued to build a program using solution state nuclear magnetic resonance (NMR) spectroscopy, molecular biology, and now computational methods to study neuropeptides. We have three main areas of activity: conformations of neuropeptides in solution; neuropeptide precursor protein three-dimensional structure determination, processing studies, and evolution; and structures of peptides bound to receptors.

This year's highlights include:

- We have made substantial progress using NMR to characterize the conformations of a subfamily of related neuropeptides in solution (manuscript submitted). In this study we compared the conformations of neuropeptides with their receptor binding affinities. The high correlation (r^2=0.93) between NMR conformational parameters and binding constants led us to propose a model called "conformational modulation." This model helps explain how the structures of neuropeptides in solution can lead to differential signaling.
- We are in the final stages of optimizing production of two neuropeptide precursor proteins. These proteins will be used for NMR structural and *in vitro* processing studies. A recent publication by Dr. Chris Li has demonstrated multiple phenotypes in a nematode when one of these precursor proteins is eliminated [Nelson, Rosoff, and Li, Science 281, 1686-1690, 1998]. We have received notice of funding by NSF to continue these studies and to collaborate with the Dr. Li on structure/function relations in this important protein.
- We are continuing efforts to study neuropeptides bound to a receptor (funded by the American Heart Association). To optimize sample conditions, we have begun several model studies, including the use of dilute gels to suspend oocyte preparations containing receptors, diffusion studies of peptides in the gels, and systematic dilution receptors in well-characterized ligand-receptor systems. We are also collaborating with Dr. Peter McGuire at UF on the generation of antibodies to the receptor, in order to aid in future sample preparations. We have ordered a liquid MAS NMR probe to help with NMR measurements.

During the past year, we had several collaborations. The most productive have been:

- Dr. Brian Cain and Paul Sorgen (UF): Analysis of the properties of the *b* subunit in F_1-ATPase (Sorgen *et al*., 1998). We used NMR to show that a region of the subunit had nascent-helical properties in solution.
- Dr. Jeff Hillman (UF): Structure of a broad spectrum antibiotic. We are using NMR to determine both the covalent and three-dimensional structure of mutacin, a small peptide antibiotic. We have used NMR to show that mutacin most likely has more than one form, suggesting the possibility of multiple biological functions.
- Dr. Ben Dunn (UF): Structure of a yeast protease inhibitor. We have assigned a 33 amino acid fragment that has potent biological activity. This molecule has strong signs of structure, the knowledge of which will facilitate the design of better inhibitors. We are producing the full-length protein with isotopic enrichment in order to eliminate overlap and solve the three-dimensional structure.
- Dr. Lou Carlacci (USF) and Dr. Hai-Ping Cheng (UF): Computational approaches to peptide conformational analysis. We have begun using Monte Carlo algorithms and Density Functional Theory calculations to calculate the distribution of structures of neuropeptides. These will be compared to experimental data, described elsewhere in this report.

The M2 Proton Channel from Influenza A Virus: Toward a Structural Characterization

Kovacs, F., NHMFL/FSU, Molecular Biophysics
Tian, C., NHMFL/FSU, Molecular Biophysics
Song, Z., NHMFL
Lamb, R., Northwestern Univ. and Howard Hughes Medical Inst.
Cross, T.A., NHMFL/FSU, Chemistry and Molecular Biophysics

The M2 protein is a small (98 amino acid residues) integral membrane protein from the viral coat of Influenza A virus. As a tetramer, it forms a proton channel with each monomer contributing a single

transmembrane helix. A combination of approaches is being brought to bear on this challenging structural problem. Typical of membrane protein systems, despite years of effort, no crystals of this protein have been reported in the literature, and hence X-ray crystallography is not applicable. Solution NMR is the other primary technique for achieving a high resolution structure, but no oligomeric proteins have been successfully studied in detergent micelle systems. The detergent micelle solubilization is necessary to achieve global isotropic motions for solution NMR studies. However, recent accomplishments in solid state NMR make this protein a tractable system for structural characterization using uniformly aligned lipid bilayer preparations. Furthermore, molecular biological techniques involving cysteine mutagenesis followed by disulfide cross-linking can be used to characterize the monomer to monomer interface.

The initial solid state NMR experiments have been performed on just the fragment of the protein that spans the lipid bilayer, a 25 amino acid residue polypeptide described as M2-TMP. This molecule is known to form proton channels with characteristics very similar to that of the intact protein. Such a protein fragment can be chemically synthesized and isotopically labeled, whereas the intact protein requires biosynthetic methods that does not permit single site labeling. Labels in the polypeptide backbone have led to preliminary structural models, in which, the helix tilt and rotational orientation is defined. Shown in Figure 1 is a recent PISEMA spectrum, in which, the ^{15}N-^{1}H dipolar interaction is resolved from the anisotropic ^{15}N chemical shift interaction. While the experimental parameters are being optimized with these single sites, or oligosite labeled samples, uniformly ^{15}N labeled samples of the intact protein have been recently prepared biosynthetically, and will be characterized by this same experiment. The relatively narrow resonance linewidths and the broad frequency range for both of these interactions should permit the collection of well resolved spectra from uniformly ^{15}N labeled M2 protein that has recently been prepared.

In the meantime, cysteine mutagenesis has been used to characterize which amino acid sites are at the monomer-monomer interface. These experiments have clearly demonstrated one of the reasons why these molecules are so difficult to crystallize. If the cross-linking is performed under standard conditions the reaction is quite non-specific. In other words the monomers possess considerable flexibility from what appears to be a weakly defined minimum energy conformation. This appears to be a typical problem in membrane proteins where there are few polar side chains and few electrostatic interactions for constraining the tertiary and quarternary structure. Instead, the dominant interactions are the very weak and non specific van der Waals interactions. However, by lowering the temperature, a much more specific pattern of residue contacts can be achieved. The combination of this monomer-monomer structural information and the high resolution structural constraints from within the monomers by solid state NMR are leading to the first experimental-based structural model of this important protein.

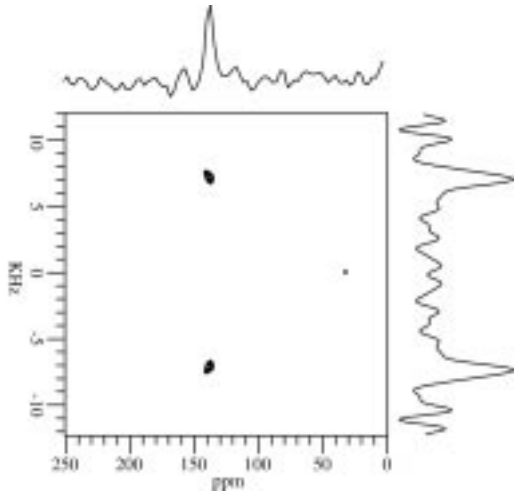

Figure 1. Solid state ^{15}N PISEMA spectra of isotopically ^{15}N-Leu$_{26}$ labeled M2-TMP. The dipolar splitting can be directly interpreted to find the orientation of the ^{15}N-^{1}H bond for this single site within the molecular structure. Note that all of the molecules in the sample give rise to the same chemical shift and the same dipolar interaction, and therefore, the sample is homogeneous and a symmetric tetramer with respect to the bilayer normal that is aligned parallel to the magnetic field direction in this sample.

Conformational Study of Adenosine Nucleotides Bound to *E. Coli.* Adenylate Kinase and Yeast 3-Phosphoglyerate Kinase by NMR Spectroscopy

Lin, Y., Indiana Univ. Purdue Univ. Indianapolis (IUPUI), Physics
Raghunathan, V., IUPUI, Physics
Nageswara Rao, B.D., IUPUI, Physics

We have been using the 720 MHz high resolution NMR spectrometer at the NHMFL to make some of the critical measurements in a NIH-funded project entitled "Active-Site Structures of ATP-Utilizing Enzymes." A brief description of the backgrounds, methodology, specific measurements performed at the NHMFL, and the results is given below.

Background and Theory: ATP-utilizing enzymes catalyze a variety of critical enzymatic reactions in biological systems. All these reactions require a divalent cation, Mg(II) *in vivo* and can be substituted by paramagnetic cations, Mn(II) and Co(II) *in vitro*. Some of the principal goals of the project is to use high resolution NMR methods to characterize the structures of nucleotides at the active sites of the ATP-utilizing enzymes. A free ATP molecule in solution has several internal motions, which are likely to be arrested in enzyme-bound complexes. To characterize such a conformation we use two methods: TRNOESY and nuclear relaxation in the presence of paramagnetic cations. The TRNOESY measurements yield the adenosine conformations, specifically, the glycosidic orientation (of the adenine base with respect to the ribose), ^{31}P relaxation measurements yields the location of cation (Co(II)) with respect to the phosphate chain, ^{13}C relaxation measurements on [ul-^{13}C]nucleotides yield the conformation of the adenosine with respect to the cation (Mn(II)), which is attached to the phosphate chain. Analysis of paramagnetic relaxation effects require measurements at several frequencies. For example, for the ^{13}C relaxation, measurement at 75 MHz and 125 MHz are made in our laboratory at IUPUI, and the NHMFL facility is used for measurements at 180 MHz.

Specific Experiments Performed at NHMFL During 1998 and Results Obtained: Measurements relevant to two enzymes were made: (1) adenylate kinase (AK), which catalyzes the reaction AMP+M(II)ATP $\xleftarrow{AK}$ ADP + M(II)ADP, and (2) 3-phosphoglycerate kinase (3-PGK) which catalyzes M(II)ATP + 3-PG $\xleftarrow{3PGK}$ M(II)ADP + 1,3-DPG. Both reactions can be activated by paramagnetic ions Mn(II) and Co(II). Previously TRNOESY and ^{31}P relaxation measurements have been made for nucleotides bound with both enzymes, which gave the conformation of adenosine moiety and the location of the metal ion with respect to the phosphate groups, respectively. The results obtained for ^{13}C relaxation at 180 MHz on [ul-^{13}C]nucleotides were analyzed along with those measured at 125 MHz and 75 MHz at IUPUI. The analysis allowed the determination of all ten Mn(II)-^{13}C distances in the enzyme-bound nucleotides. These data were used, together with the previously determined conformation of adenosine and metal-phosphate distances, to obtain a complete characterization of the conformation of the nucleotide complexed with AK and 3-PGK.

The nucleotide structures obtained represent the first such complete structural characterization made for ATP-utilizing enzymes. These structures will be correlated with the protein environments at the active sites thereby gaining insights into the mechanisms of theses reactions.

Analysis of Transdermal Drug Delivery via Electroporation and Iontophoresis Using Pulsed Field Gradient Nuclear Magnetic Resonance

Locke, B.R., FAMU-FSU College of Engineering
Moerland, T.S., FSU, Biology
Caban, J., FSU, Molecular Biology
McFadden, L., FSU, Biology
Gibbs, S.J., NHMFL/FAMU-FSU College of Engineering

Recent studies have indicated that transdermal drug delivery can be enhanced by the application of electrical fields, however, a detailed understanding of the mechanism by which electrical fields affect transport in skin is not available. Therefore, the present study was conducted, through support by the Whitaker Foundation, to use magnetic resonance methods to elucidate transport pathways and skin structure when electrical fields are applied to skin.

Magnetic resonance images and maps of water self-diffusion coefficients of the skin of hairless rats under three conditions of (1) no electrical field, (2) 0 V to 20 V constant electrical fields, and (3) 220 V 1 ms pulsed electrical fields were obtained by MR microscopy. The no-voltage cases provided controls for the electrical field experiments, and also showed that high resolution images (20 μm x 20 μm x 200 μm) could be obtained and that the basic structural features of the skin, including hair follicles, viable epidermis, dermis, and sebaceous glands, can be identified clearly in MR images of skin. In addition, these results showed that water diffusion coefficients in the hair follicle and viable epidermis regions were less than 30% of free solution values, and generally diffusion in the hair follicle regions was higher than that in the viable epidermis. Experiments with applied constant voltages indicated that skin structure was not dramatically altered until the voltage was 20 V, where a significant expansion of the viable epidermal region of the skin was observed. Water diffusion was increased in both regions of the skin when the field was applied. High voltage pulsed electrical fields showed dramatically increased hydration of the upper layer of cells in the skin, i.e. the stratum corneum, and, furthermore, that the water diffusion coefficients in the dermis and hair follicles increased about 30% when the field was applied.

These results are important since they demonstrate the applicability of MR microscopy for measurement of structure and transport in tissue with applied electrical fields. In combination with a mathematical model of the various transport pathways in the skin, these results also define quantitatively the range of molecules (in terms of size and hydrophobicity) that can transport across the skin, and what pathways these molecules will take through the skin when electrical fields are applied. As voltage is increased transport through follicle regions is favored for a broader range of molecular solutes.

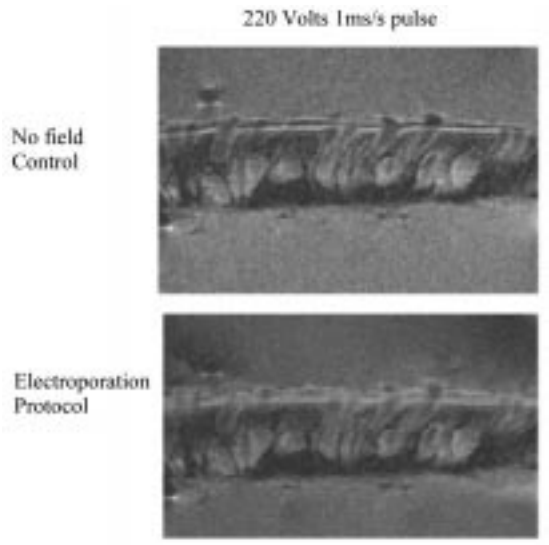

Figure 1. Magnetic resonance images of skin at a resolution of 19.5 x 19.5 microns.

^{19}F NMR Studies of 5-F Tryptophan Labeled Human Soluble Tissue Factor

Luck, L.A., Clarkson Univ., Chemistry and Biology
Rusinova, E., Clarkson Univ., Biology
Zemsky, J., Clarkson Univ., Biology
Ross, J.B.A., Mt. Sinai School of Medicine
Logan, T.M., NHMFL/FSU, Chemistry

^{19}F NMR was used to investigate the local environments of the four Tryptophan (Trp) residues of the extracellular domain of human tissue factor (sTF) using 5-F-Trp as a probe. Replacement of the Trp residues by this analogue had no effect on biological activity. Individual ^{19}F resonances were assigned using a series of Trp to Phe single mutants. At 25 °C, W14 and W45 overlap, but become resolved as the temperature increases to 40 °C due to line narrowing from the reduced rotational correlation time at the higher temperature. CD studies confirmed that the protein remained folded in the native conformation at 40 °C. Solvent-induced isotope shifts were used to investigate surface exposure of individual Tryptophan residues, indicating the W5 was the only Tryptophan residue with significant solvent exposure. These results were confirmed by paramagnetic broadening studies. When Gd-EDTA and Gd-DPTA were added to the solution containing sTF, W5 resonance was broadened significantly, while the others were essentially unaffected. We also investigated the macromolecular interactions in the binary sTF-VIIa complex using ^{19}F NMR spectroscopy as a prelude to more detailed conformational studies of the complex.

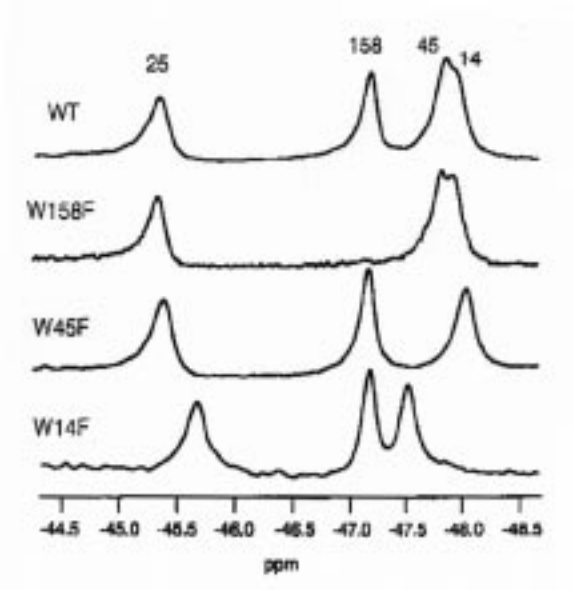

Figure 1. Example of chemical shift assignments for fluorotryptophan by site-directed replacement of tryptophans by phenylalanine.

Studies of Apolipoprotein C-II Structure

Maguire, B.C., FSU, Molecular Biophysics
Murali, N., NHMFL
Gaffney, B.J., NHMFL/FSU, Biology and Molecular Biophysics

Apolipoprotein C-II (Apo C-II) is a member of the class of proteins called apolipoproteins. These proteins are found on the surface of lipoprotein particles in blood. The apolipoproteins perform many tasks, including activation of enzymes that act on lipid substrates present in lipoproteins, and binding to receptors that clear lipoproteins from the bloodstream. Apo C-II is an activator of lipoprotein lipase, an enzyme that hydrolyzes dietary triglycerides (fats).

Research in our lab has focused on solution state NMR techniques for structural studies of Apo C-II. The isotopically-labeled protein of 79 amino acid residues was obtained from a bacterial expression system. Figure 1 presents an expanded region from an HSQC spectrum of 1.5 mM Apo C-II in a solution containing 200 mM sodium dodecyl sulfate (SDS). The SDS forms small micelles that mimic the lipid environment on the surface of lipoproteins. The separation of resonances in this experiment demonstrates that a structure of Apo C-II can be determined using further multidimensional NMR experiments.

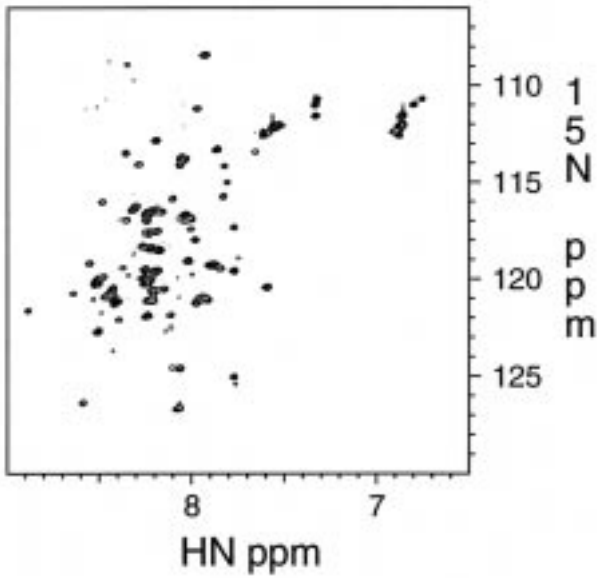

Figure 1: An expanded region of an HSQC spectrum of 1.5 mM Apo C-II in 200 mM SDS, 0.15 M sodium chloride, 20 mM sodium phosphate, 1 mM DSS is shown. The spectrum was recorded at 35 C, and an operating frequency of 720 MHz. The expanded region contains all of the expected peaks with the exception of one from the ring proton of Trp 26, which is well removed from these peaks and is excluded for the sake of resolution.

Application of Micro-Electrospray Liquid Chromatographic Techniques to FT-ICR MS to Enable High-Sensitivity Biological Analysis

Marshall, A.G., NHMFL/FSU, Chemistry
Emmett, M.R., NHMFL
White, F.M., FSU, Chemistry
Shi, S.D.-H., FSU, Chemistry
Hendrickson, C.L., NHMFL

A microbore electrospray (ESI) injection system has been adapted to our 9.4 T ESI FT-ICR mass spectrometer, greatly enhancing the stability and sensitivity of the system. Spray was generated from micro-ESI needles made from sharply tapered, polished fused silica capillaries of 25 μm to 50 μm inner diameter. Micro-ESI permits low-level sample analysis by constant infusion at sub-μL/min flow rate over a wide range of solvent conditions in both positive and negative ion mode. The system is flexible, and allows rapid conversion to allow routine LC/MS analysis on low-level mixtures presented in biological media. LC/MS analyses were accomplished by replacing micro-ESI needles with capillaries packed with reverse phase retention media to permit analyte concentration and purification prior to analysis (micro-ESI/LC). A unique nano-flow LC pumping system was developed, capable of producing a true unsplit solvent gradient at flow rates below 1 μL/min. The micro-ESI/LC FT-ICR system produces mass spectra from a mixture of three neuroactive peptides at a concentration of 500 attomol/μL (5 fmol each total loaded) in biological salts with baseline separation, signal-to-noise ratio of >10:1, and mass resolving power >5,000. These results represent a reduction in detection limit by a factor of ~2 x 10^6 over the best previously published LC/FT-ICR MS data.

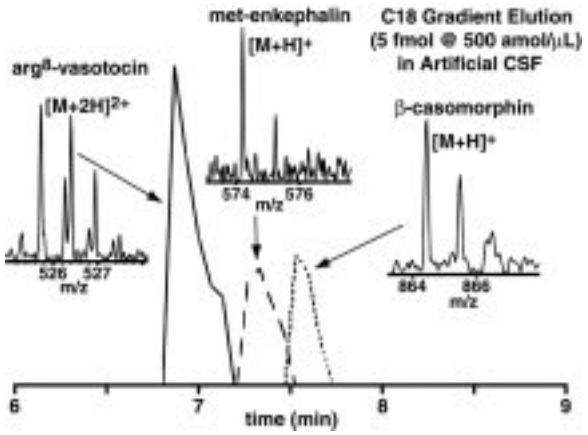

Figure 1. True gradient elution of 5 fmol each of an equimolar mixture of three peptides: Arg^8-vasotocin, methionine enkephalin, and β–casomorphin. Samples were dissolved in artificial cerebrospinal fluid at 500 attomol/μL each and loaded (10 μL) onto a C18 packed micro-ESI needle. The reconstructed ion chromatogram is shown below, with ESI FT-ICR mass spectra of individual peptide spectra shown as insets.

Reference:

1 Emmett, M.R., J. Am. Soc. Mass Spectrom., 9, 333-340 (1998).

Conformational and Dynamic Changes of *Yersinia* Protein Tyrosine Phosphatase Induced by Ligand Binding and Active Site Mutation, and Revealed by H/D Exchange and Electrospray Ionization Fourier Transform Ion Cyclotron Resonance Mass Spectrometry

Marshall, A.G., NHMFL/FSU, Chemistry
Wang, F., NHMFL
Li, W., FSU, Chemistry
Emmett, M.R., NHMFL
Hendrickson, C.L., NHMFL
Zhang, Y.-L., Albert Einstein College of Medicine
Wu, L., Albert Einstein College of Medicine
Zhang, Z.-Y., Albert Einstein College of Medicine

Protein tyrosine phosphatases (PTPase) play important roles in the intracellular signal transduction pathways that regulate cell transformation, growth, and proliferation. We have determined solvent accessibility for backbone amide protons from various segments of wild-type *Yersinia* (bubonic plague) PTPase in the presence or absence of 220 μM vanadate, a competitive inhibitor, as well as an active site mutant in which the essential cysteine 403 has been replaced by serine (C403S). The method consists of solution-phase H/D exchange, followed by pepsin digestion, high-performance liquid chromatography, and electrospray ionization high field (9.4 T) FT-ICR mass spectrometry. Proteolytic segments spanning ~93.5% of the primary sequence are analyzed. Binding of vanadate reduces H/D exchange rate throughout the protein, both for the WpD loop and for numerous other residues that are shielded when that loop is pulled down over the active site on binding of inhibitor. The active site C403S mutation reduces solvent access to the WpD loop itself, but opens up the structure in several other segments. Collectively, these results establish the flexibility of the WpD loop (previously inferred by comparing PTPase x-ray single-crystal diffraction structures in presence and absence of tungstate inhibitor), as well as several other significant changes in segment exposure and/or flexibility that are not evident from x-ray structures.

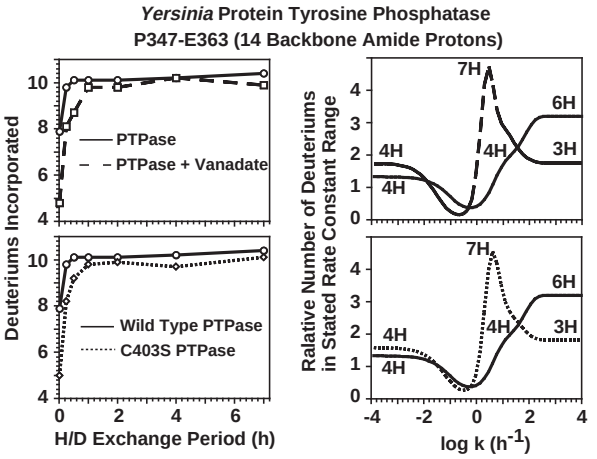

Figure 1. H/D exchange time courses (left) of segment P347-E363 (14 backbone amide protons) from wild-type PTPase (○), wild-type PTPase plus vanadate (□), and C403S PTPase (◇), analyzed by MEM to yield their H/D exchange rate constant distributions (right) for wild-type PTPase (——), wild-type PTPase plus vanadate (– – – –), and C403S PTPase (·····). The number of backbone amide hydrogens for each resolved peak in the MEM-derived rate constant distribution is shown above that peak.

Reference:

1 Wang, F., *et al.*, Biochemistry 37, 15289-15299 (1998).

Gas Phase RNA and DNA Ions. H/D Exchange of the $[M - H]^-$ Anions of Nucleoside 5'-Monophosphates (GMP, dGMP, AMP, dAMP, CMP, dCMP, UMP, dTMP), Ribose-5-Monophosphate (R5P), and 2-Deoxyribose-5 Monophosphate (dR5P) with D_2O and D_2S

Marshall, A.G., NHMFL/FSU, Chemistry
Freitas, M.A., NHMFL
Shi, S.D.-H., FSU, Chemistry
Hendrickson, C.L., NHMFL

H/D exchange from D_2O and D_2S to electrosprayed $[M - H]^-$ nucleoside 5'-monophosphate anions (GMP, dGMP, AMP, dAMP, CMP, dCMP, UMP, TMP) has been examined by Fourier transform ion cyclotron resonance mass spectrometry at 9.4 T, along with sugar phosphate controls (ribose-5-monophosphate (R5P), and 2-deoxyribose-5-monophosphate (dR5P)).[1] The relative exchange rates of the nucleotides with D_2O were: dR5P > dCMP > R5P > CMP > dAMP > UMP > AMP > dTMP >> dGMP >> GMP, and with D_2S: CMP > UMP ≈ dTMP > dCMP > dAMP > AMP > R5P > dR5P >> dGMP >> GMP. All exchange rates increase dramatically on changing from D_2O to D_2S, due to the smaller gas phase acidity difference between exchange reagent and the nucleotide: $\Delta(\Delta H_{acid}) > 60$ kcal mol^{-1} for D_2O *vs.* $\Delta(\Delta H_{acid}) > 20$ kcal mol^{-1} for D_2S. *Ab initio* calculations on model compounds at the MP2/6-31+G*//HF/6-31+G* level yield the following order of calculated acidities for each of the exchangeable hydrogens: $R_2O_3PO\text{-}H$ > $R_2N\text{-}H$ > (R_2O-H on ribose) > $RN\text{-}H_2$ > (R_2O-H on 2-deoxyribose). The present results provide a quantitative measure of proton exchange rates, in minutes for D_2S (rather than hours for D_2O) for gas-phase nucleotide anions, thereby opening up a wide range of extensions to chemically modified nucleotides as well as single-stranded and duplex RNAs and DNAs.

These results have been featured by *Analytical Chemistry*.[2]

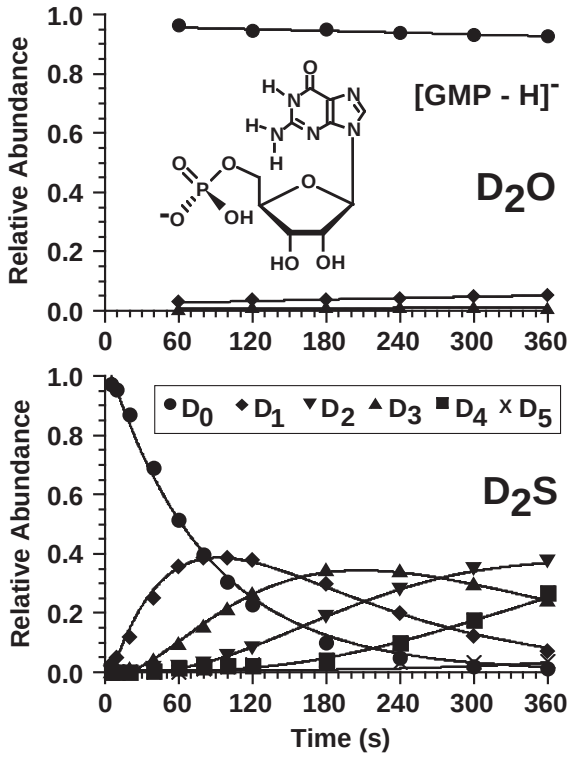

Figure 1. Reaction progress curves for guanosine 5'-monophosphate reacting with (top) D_2O at 5 x 10^{-8} torr, and (bottom) D_2S at 5 x 10^{-8} torr. Note the faster and more complete reaction with D_2S.

References:

1 Freitas, M.A., *et al*., J. Am. Chem. Soc., 120, 10187-10193 (1998).
2 Anal. Chem., 70, 767A (1998).

High Field FT-ICR Mass Spectrometry for Simultaneous Trapping and Gas Phase Hydrogen/Deuterium Exchange of Peptide Ions

Marshall, A.G., NHMFL/FSU, Chemistry
Freitas, M.A., NHMFL
Hendrickson, C.L., NHMFL
Emmett, M.R., NHMFL

Gas-phase hydrogen/deuterium exchange, of D_2O with $[M + H]^+$ ions of angiotensin II, angiotensin I, [Sar^1]-angiotensin II, bradykinin, des-Arg^1-bradykinin, des-Arg^9-bradykinin, luteinizing hormone releasing hormone (LH-RH) and substance P, has been examined by Fourier transform ion cyclotron resonance mass spectrometry at 9.4 T. Because FT-ICR dynamic range increases quadratically with magnetic field, parent ions from a mixture of several peptides may be confined simultaneously for long periods at high pressure (e.g., 1 h at 1 x 10^{-5} torr) without quadrupolar axialization (and its attendant ion heating), for faster data acquisition and better controlled comparisons between different peptides. High magnetic fields also facilitate SWIFT isolation of monoisotopic $[M + H]^+$ parent ions, so that deuterium incorporation patterns may be determined directly without the need for isotopic distribution deconvolution. Finally, higher magnetic fields provide for greatly extended trapping periods, for measurement of much slower rates. Angiotensin I, angiotensin II, and [Sar^1]-angiotensin II are found to undergo rapid exchange. Angiotensin II and [Sar^1]-angiotensin II exhibit multiple deuterium uptake distributions, corresponding to multiple gas-phase conformations. In contrast, substance P exchanges slowly, and LH-RH displays no observable exchange. Comparison of the relative H/D exchange rates for bradykinin, and its des-Arg-derivatives supports the hypothesis that bradykinin adopts a folded gas-phase conformation that unfolds upon removal of either terminal arginine residue.

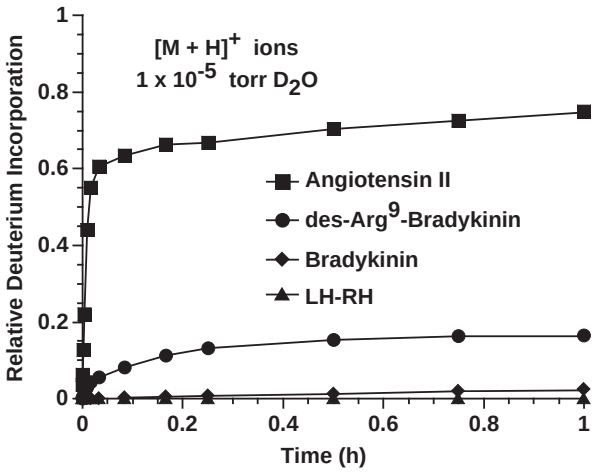

Figure 1. Deuterium incorporation vs. time profiles for gas-phase simultaneous H/D exchange of angiotensin II, bradykinin, des-Arg^9-bradykinin, and LH-RH with D_2O (1 x 10^{-5} torr).

Reference:

1 Freitas, M.A., *et al*., J. Am. Soc. Mass Spectrom., 9, 1012-1019 (1998).

World's Highest-Resolution Mass Spectrometer Can Count the Number of Sulfur Atoms in a Protein

Marshall, A.G., NHMFL/FSU, Chemistry
Shi, S.D.-H., FSU, Chemistry
Hendrickson, C.L., NHMFL

A typical molecular ion mass spectrum consists of a sum of signals from species of various possible isotopic compositions. Only the "monoisotopic" peak (e.g., all carbons are ^{12}C; all nitrogens are ^{14}N, etc.) has a unique elemental composition; each other "isotope" peak at approximately integer multiples of ~1 Da higher in mass includes contributions from isotope combinations differing by a few mDa (e.g., $^{13}C_2$ or $^{15}N_2$ or $^{13}C^{15}N$ or ^{34}S or ^{18}O, etc., each ~2 Da above the monoisotopic mass).

Ph.D. candidate Stone Shi, working with Christopher Hendrickson, and Alan Marshall at

the NSF National High Field FT-ICR Mass Spectrometry Facility at Florida State University, recently reported the first resolution of isotopic "fine structure" for proteins up to 15.8 kDa (^{13}C,^{15}N doubly-depleted p16 tumor suppressor protein), achieved by electrospray ionization followed by ultrahigh resolution Fourier transform ion cyclotron resonance mass analysis at 9.4 T.[1] Moreover, a new record high mass resolving power of 8,000,000 for a protein was demonstrated on bovine ubiquitin (8.6 kDa). These results represent a ten-fold increase in the highest mass at which isotopic fine structure had previously been reported. Because isotopic fine structure reveals elemental composition directly, it can be used to confirm or determine molecular formula. For example, we were able to determine the correct number (5) of sulfur atoms in p16 solely from the abundance ratio of the resolved 34S peak to the monoisotopic peak (see Figure 1).

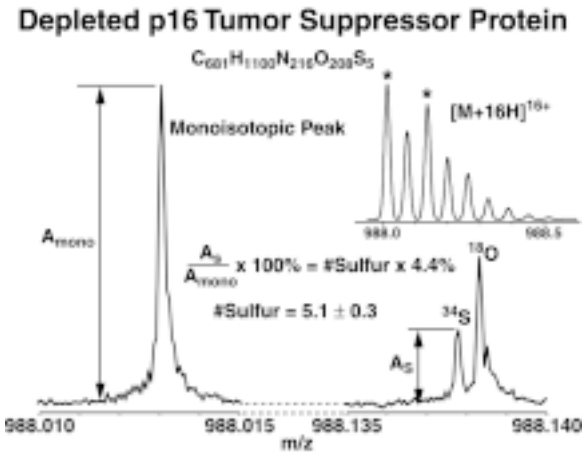

Figure 1. Mass-scale expanded electrospray FT-ICR mass spectra of two isotopic peaks of ^{13}C, ^{15}N doubly depleted p16 tumor suppressor protein. In the theoretical isotopic distribution shown at upper right, stars denote the monisotopic peak (left), and isotopic peak (right) ~2 Da above the monoisotopic mass. From the abundance ratio of the (resolved) ^{34}S to the monoisotopic species (bottom), we determined the number of sulfur atoms in the protein as 5.1 ± 0.3 without use of any other information about the protein.

Immediately after its publication, this achievement was featured in *Chemical & Engineering News*[2] and *Analytical Chemistry*.[3]

References:

1 Shi, S.D.-H., *et al.*, Proc. Natl. Acad. U.S.A., 95, 11532-11537 (1998).
2 Chemical & Engineering News, 76, 36 (1998).
3 Anal. Chem., 70, 702A (1998).

Transgenic Arabidopsis Plants as Monitors of Low Gravity and Magnetic Field Effects

Meisel, M.W., UF, Physics/NHMFL
Paul, A.-L., UF, Horticultural Sciences and the Biotech. Program
Ferl, R.J., UF, Horticultural Sciences and the Biotech. Program
Stalcup, T.F., FSU, Physics/NHMFL
Reavis, J., FSU, Physics/NHMFL
Brooks, J.S., FSU, Physics/NHMFL

A number of problems must be solved before humans will be able to spend long periods of time in space. One major issue is the establishment of a sustainable food supply since plants cultivated in low gravity possess drastically reduced growth characteristics. Long term Earth-based testing would contribute to our understanding of plant growth in low-g conditions and would help optimize the design of experiments that will eventually fly on the space shuttle. Magnetic levitation is an established technique[1] that can supply the longest-term Earth-based low-g environment.

Three arabidopsis plants[2] (4 weeks old) were magnetically levitated for a period of 2.3 hours. This growth window represents a significant fraction of the development time of arabidopsis. The results are shown in Figure 1.

Our experiments qualitatively suggest the arabidopsis plants were differentially stressed by the high magnetic field and low-g environments. For plants, such a significant response to the presence of a strong magnetic field has not been reported. It appears that low gravity environmental effects may be induced by magnetic levitation,

albeit on a "background" response generated by the strong magnetic field. The magnetic effects need to be studied and understood if high magnetic field MRI is going to be used to image *in vivo* gene regulation.[3]

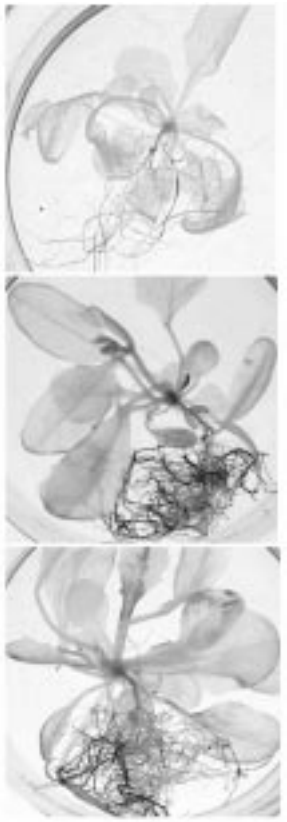

Figure 1. Stained intact plants after 2.3 hours of: (top) B ≤ 0.1 mT, (center) B = 18.9 T and B∇B ≈ 0, and (bottom) magnetic levitation in B = 14.4 T and B∇B = 1708 T^2 m^{-1}. The plants in the large magnetic fields (center and bottom) show stress response as indicated by the blue (i.e. dark) stain, while the low field control (top) shows significantly weaker response. The levitated plants (bottom) possess a higher level of expression of the reporter gene than the specimens in the constant magnetic field (center). A full color version of this figure is available at *http://www.phys.ufl.edu/~meisel/arabexp.htm.*

The Space Biology program of R.J. Ferl is supported by NASA (NAG 10-0145).

References:

1 Berry, M.V., *et al.*, Euro. Jour. Phys., 18, 307 (1997).
2 Meinke, D.W., *et al.*, Science, 282, 662 (1998).
3 http://www.magnet.fsu.edu/NMRcoll/ index.html

Dynamics of Phosphorous Metabolites in Striated Muscle

Moerland, T.S., FSU, Biology
Vanderlinde, O.H., FSU, Biology
Carbone, F.A., FSU, Biology

This research comprises two projects that employ NMR to investigate biological function in intact cellular systems. The projects are (1) a systematic investigation of the intracellular diffusive mobility (D) of an energetically important phosphorous metabolite (phosphocreatine, PCr) in skeletal muscle, and (2) measurements of the time-course of metabolic recovery in muscle after a bout of contractile activity. The goals of these projects are to (1) attain a better understanding of the effects of cellular ultrastructure on the intracellular diffusive mobility of small metabolites, and (2) to understand the determinants of post-contraction recovery in muscle. Experiments in both areas utilize the wide-bore 600 MHz Bruker DMX nuclear magnetic resonance spectrometer at the NHMFL. Because of its singular combination of sensitivity and wide bore, this system is uniquely suited for analysis of physiological transients in living tissue.

Work in the first area has shown that intracellular diffusion of small solutes, such as PCr, is highly anisotropic in skeletal muscle. Diffusion across the radius of these cylindrically shaped muscle cells is restricted to a far greater extent than is diffusion along the long axis of these cells. Mathematical analysis shows that this result is best explained by structures with lengths of several μm, such as mitochondria and the sarcoplasmic reticulum . The time-course, over which restricted diffusion is manifest, is too brief to be consistent with solute interaction with the cell membrane, which has a radius of ~ 50 μm (Figure 1), and too long to be consistent with interaction with the nm-scale lattice of contractile proteins in muscle.

Experiments in the second project area utilize this capability to understand the effects of diabetes on metabolism in skeletal muscle. Post-contraction

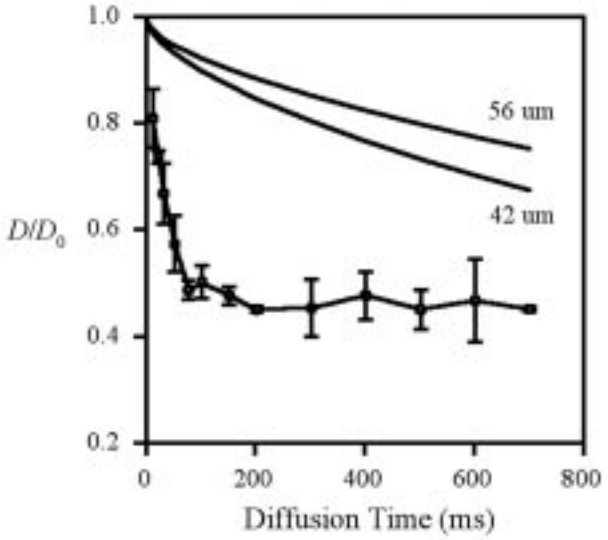

Figure 1. Relative diffusion coefficient of PCr as a function of diffusion time in muscle cells. PCr diffusion in the radial direction is rapidly attenuated with time, which is indicative of restricted diffusion. Solid lines show the results of mathematical simulations of interaction with the cell membrane.

recovery of phosphorous metabolites are monitored in single mouse muscles with a temporal resolution of ~ 16 seconds. The data show that insulin-dependent diabetes significantly slows the ability of both fast and slow types of muscle to recover after contraction.

This work is supported by NSF IBN-98-08120.

Spliceosomal RNA-RNA Interactions: Structural Characteristics of the Eukaryotic U2snRNA-Intron Branch Site Pairing

Newby, M.I., NHMFL/FSU, Chemistry and Molecular Biophysics
Greenbaum, N.L., NHMFL/FSU, Chemistry and Molecular Biophysics

The removal of non-coding sequences (introns) from eukaryotic precursor mRNA occurs via specific RNA-protein and RNA-RNA interactions in the spliceosome. One such RNA-RNA interaction involves the U2 small nuclear (sn) RNA and the branch site of the intron, whose pairing results in the bulging of an adenosine residue. The 2'OH of this adenosine is known to be critical in the first step of splicing. Structural features of this RNA-RNA pairing are being examined by solution NMR spectroscopy in order to elucidate the role of the branch site adenosine in splicing activity. Nine- and ten-nucleotide fragments representing the U2 and intron sequences, respectively, were chemically synthesized and deprotected by standard phosphoramidite methods, and were purified by HPLC. Imino-imino and imino-amino crosspeaks observed in two-dimensional NOESY spectra of exchangeable protons indicate stable base pairing consistent with the predicted secondary structure. Base-ribose connectivities observed in NOESY spectra of nonexchangeable protons are consistent with a predominantly A-form helical structure. A resonance at approximately 8.4 ppm, downfield from the remaining aromatic resonances, has been tentatively identified as the H8 proton belonging

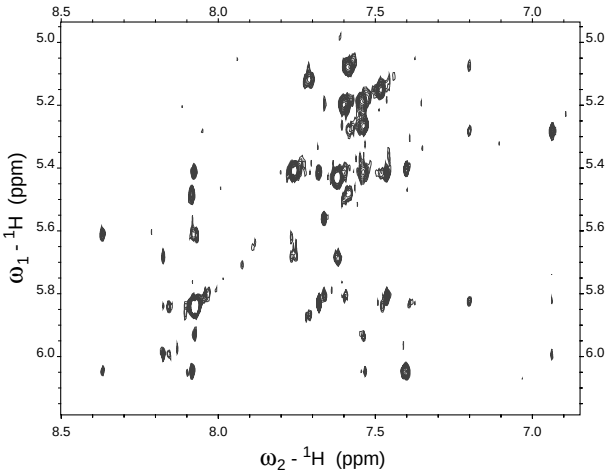

Figure 1. Region of a NOESY spectrum of nonexchangeable protons of the U2-intron construct displaying crosspeaks between RNA base and ribose H1' protons. The resonance at 8.4 ppm has been tentatively assigned as the H8 of the extrahelical adenosine involved in the first step of pre-mRNA splicing. The sample is ~1mM RNA in 10 mM sodium phosphate, pH 6.3, 75 mM NaCl, 0.1 mM EDTA, in D_2O, at 20 °C. The spectrum was acquired on the 720 MHz Varian Unity Plus spectrometer at the NHMFL with a mixing time of 350 ms.

to the branch site adenosine that is responsible for the cleavage event of the first step of splicing. The U2-intron pairing has also been studied in the presence of cobalt (III) hexamine, which mimics hydrated magnesium ion. Adenine H2 resonances are not shifted upon addition of metal, and base pairing is not disrupted, suggesting that there is no global conformational change induced. However, the 8.4 ppm H8 resonance is slightly upfield shifted upon addition of cobalt (III) hexamine, suggesting the proximity of this proton to a metal coordination site created by a bulged base. These data support the model of an extrahelical branch site adenosine accessible for recognition by a splice donor site.

Distance Changes Within the Myosin Head in Pre- and Post-Power Stroke States

Palm, T., NHMFL
Brown, L., Univ. of Sydney, Australia, Pathology
Li, H.-Ch., NHMFL
Sale, K., NHMFL/FSU, Biological Sciences
Hambly, B., Univ. of Sydney, Australia, Pathology
Fajer, P.G., NHMFL/FSU, Biological Sciences and Institute for Molecular Biophysics

The relative movement of the motor and regulatory domains of the myosin head is likely to be the force generating conformational change in the energy transduction of muscle (Rayment *et al*., 1993). To test this model we have measured three distances between the catalytic domain and regulatory domains and within the regulatory domain of myosin using frequency modulated FRET in the intermediate states of myosin ATPase cycle. The donor/acceptor pairs included: cys707 and cys177 of LC1(38A from x-ray structure); cys177-LC1 and cys154 of RLC (46A); cys177-LC1 and cys108 of gizzard RLC (33A). The IAEDANS (donor) or acceptor (DABMI, IAF) labeled light chains (LC1, RLC) were exchanged into monomeric myosin and the distances were measured in the putative pre-power stroke states (in the presence of MgATP, or ATP/AlF4-) and the post-power stroke states (ADP and the absence of nucleotides). For each of the three distances the donor/acceptor pairs were usually reversed to avoid potential problems arising from unknown orientational factors. In all cases, the distances did not vary by more than 2 Å putting strong constraint on the extent of conformational changes. The maximum axial movement of the distal part of myosin head was modeled assuming various fulcrum points suggested by crystal structure of the myosin head.

Prediction of Spin Label Orientation in the Crystal Structure of Proteins

NHMFL

Sale, K.L., NHMFL/FSU, Biological Sciences
Sharp, K.A., Univ. of Pennsylvania, Biochemistry
Fajer, P.G., NHMFL/FSU, Biological Sciences and Institute for Molecular Biophysics

Knowledge of the orientation of a nitroxide spin label within a protein is essential to the interpretation of EPR spectra in terms of the orientation of the labeled protein within a macromolecular complex. Thus, we have developed a strategy for determining the orientation of the nitroxide probe within a protein via direct modeling of the probe environment. A series of spin labels of varying size and structure were docked to each of several sites within the myosin head crystal structure. The "modified" structure was annealed, and an exhaustive search over conformational space was performed using XPLOR® to obtain the most probable orientation of the spin label within the binding pocket. The predicted conformation was compared to the orientation of the label obtained from the spectra of myosin heads in an ordered system. Good qualitative agreement was obtained for several spin labels with different principal axes geometry.

Compact EPR Resonator for Perpendicular and Parallel Orientation of Longitudinal Aqueous Samples

Sienkiewicz, A., State Univ. of New York at Albany, Chemistry, and Polish Academy of Sciences
Fajer, P.G., NHMFL/FSU, Biological Sciences and Institute for Molecular Biophysics
Jaworski, M., Polish Academy of Sciences
Hansen, R.E., Update instrument, Inc.
Scholes, C.P., State Univ. of New York at Albany, Chemistry

Most of the conventional EPR spectrometers employ rectangular or cylindrical resonators having an intense magnetic component (B_1) oriented perpendicular to the external Zeeman field (B). Thus, in order to obtain a high S/N, aqueous longitudinal samples are usually oriented perpendicular to the external magnetic field. In the case of spin-labeled muscle cell protein molecules, the EPR spectra reveal a strong dependence on the orientation of the muscle fiber axis relative to the external magnetic field. We present a novel Dielectric Resonator (DR)-based resonant structure that is capable to accommodate longitudinal aqueous samples in both perpendicular and parallel orientations. The resonant structure consists of two commercially available MuRata-Erie X-band DRs that are separated by a Rexolite spacer. This spacer is used for tuning the resonator to the desirable frequency and to provide for the parallel access for longitudinal samples (capillaries). A quartz capillary of 0.6 mm I.D. containing aqueous solution of IASL spin label (6.25 μM) was used for preliminary tests. Depending on the spacing between the DRs, the S/N ratios were approximately 2 to 2.5 times smaller for the parallel orientation than for the regular perpendicular sample insertion. These results are in good agreement with the theoretically estimated resonator Q- and filling factors for electric (E_1) and magnetic (B_1) components for both sample orientations. Preliminary EPR measurements performed on IASL-labeled myosin filaments revealed better S/N ratios than that obtained with the use of a modified TM_{110} cavity.

Cation Transport - Structural Based Selectivity and Efficiency

Tian, F., NHMFL/FSU, Chemistry
Miller, C., Brandeis University, Howard Hughes Medical Inst.
Wang, J., NHMFL/FSU, Chemistry
Fu, R., NHMFL
Cross, T.A., NHMFL/FSU, Chemistry and Molecular Biophysics

Two primary questions surround much of the research on ion channels; how is cation selectivity achieved, and how is efficient conductance achieved while maintaining selectivity. The highest resolution membrane protein, or polypeptide, structural characterization yet achieved by any method is gramicidin A, determined from solid state NMR derived orientational constraints of its monovalent cation selective channel state.[1] While gramicidin A is a model ion channel, recently the first crystal structure of an ion channel has been published, the K^+ channel from *Streptomyces lividans* at a modest 0.32 NM resolution.[2] Many aspects of these important questions can be addressed through the high resolution structure of gramicidin A, and provide clear predictions for the function of many other ion channels including the K^+ channel.

It has been shown through the collection of orientational constraints from dipolar interactions in the presence and absence of cations that there is very little structural change upon cation binding. In fact, the amide groups, which line the cation conducting pathway, change their orientation with respect to the channel axis by less than 2° in all cases except for two sites that tilt by as much as 4°. It can also be seen from the chemical shift results (see Figure 1) that sites that interact with the cations display a significant change in frequency, which is primarily due to a polarizability effect on the chemical shift tensor. These results lead us to the conclusion that the cation-binding site is delocalized over several amide groups, thereby forming a shallow potential energy well for cation binding. As a result the cation is not trapped in a deep well that could be generated if an ideal

binding site had been formed as had been predicted by molecular dynamics calculations. This shallow surface implies that the cation can easily be moved out of the binding site and through the channel. The delocalized nature of the binding site also suggests that the entropic penalty associated with binding has been minimized since the cation still has mobility while it is in the channel.

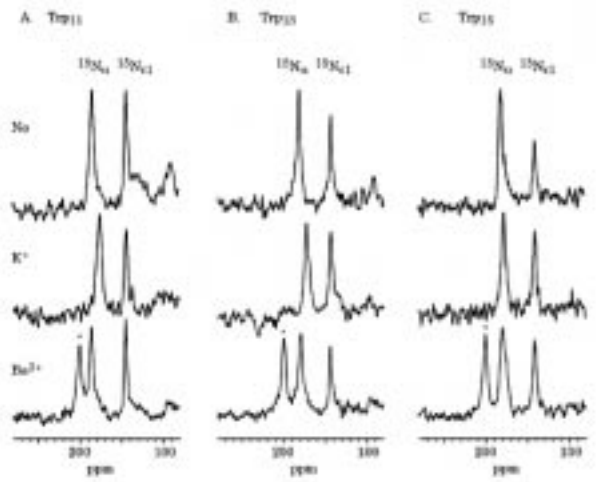

Figure 1. Comparison of K^+ and Ba^{++} effects on the ^{15}N chemical shift spectra of $^{15}N_{\alpha,\varepsilon 1}$ labeled gramicidin A in aligned hydrated lipid bilayers. Samples for the Ba^{++} studies contained the additional ^{15}N label in the Ala_3 position. While K^+ induced significant changes in the observed $^{15}N_a$ chemical shift of Trp_{11}, Trp_{13} and Trp_{15}, Ba^{++} only effects the $^{15}N_a$ chemical shift of Trp_{13} and Trp_{15}. Both $^{15}N_{e1}$ chemical shifts of side chains and $^{15}N_a$ chemical shifts of Ala_3 are unaffected by cation binding. Spectra were obtained at 40 MHz (9.4 T) at the NHMFL. * signal from $^{15}N_a$-Ala_3 gramicidin A.

Modeling of water molecules around the cation while in this binding site has shown that the volume is characterized by having at least three water molecules in the primary solvation sphere of the cation at all times. In fact, the larger monovalent cations bind closer to the channel surface so that this rule remains true. To pass through the channel this number of water molecules must be reduced to two, implying that the binding site boundary towards the inner part of the channel is defined by the position at which the third water must be stripped from the cation. This is the most costly water to remove in energetic terms. For gramicidin the presence of three flexible ligands (i.e. the waters) in the binding site explains the observed lack of specificity among the monovalent cations. It is anticipated that the K^+ channel, which has much more specificity among the monovalent cations, will show a rigid binding site, but will possess only two waters in the primary solvation sphere. The deeper potential energy well in the K^+ channel would be a problem for efficient conduction if it were not for the fact that a second cation-binding site is much closer to the primary site in the K^+ channel than in gramicidin. Therefore, efficiency and selectivity result from a careful balance of the non-covalent interactions in the channel.

References:

1 Ketchem, R.R., *et al.*, Structure, 5, 1655-1669 (1997).
2 Doyle, D.A., *et al.*, Science, 280, 69-77 (1998).

Expression and Assignment of the ^1H, ^{15}N, and ^{13}C Resonances of the C-Terminal Domain of the Diphtheria Toxin Repressor

Twigg, P.D., FSU, Molecular Biophysicis
Wylie, G.P., NHMFL/FSU, Chemistry
Wang, G., NHMFL/FSU, Chemistry
Caspar, D.L.D., FSU, Molecular Biophysicis
Murphy, J.R., Boston Univ. Medical School
Logan, T.M., NHMFL/FSU, Chemistry

The diphtheria toxin repressor (DtxR) is an iron-activated protein that functions as a global regulator of iron-sensitive genes in *Corynebacterium diphtheriae*. DtxR contains 226 amino acid residues per monomeric unit that fold into two structural domains separated by a linker. The N-terminal domain provides the DNA binding and dimer interfaces, as well as the binding sites for divalent metals. In contrast, the structure and function of the C-terminal domain are less well defined. We are using multidimensional heteronuclear NMR to determine the structure of the C-terminal domain in solution as a prelude to functional studies. Here we report the

complete, sequential ^{1}H, ^{15}N, and ^{13}C resonance assignments for the C-terminal domain (residues N130-L226) of DtxR. Figure 1 shows the 2D ^{1}H-^{15}N HSQC spectrum collected on a 2 mM sample of ^{15}N-labeled DtxR(130-226). Except for N207, all resonances have been assigned, accounting for all the backbone and sidechain amides of DtxR(130-226).

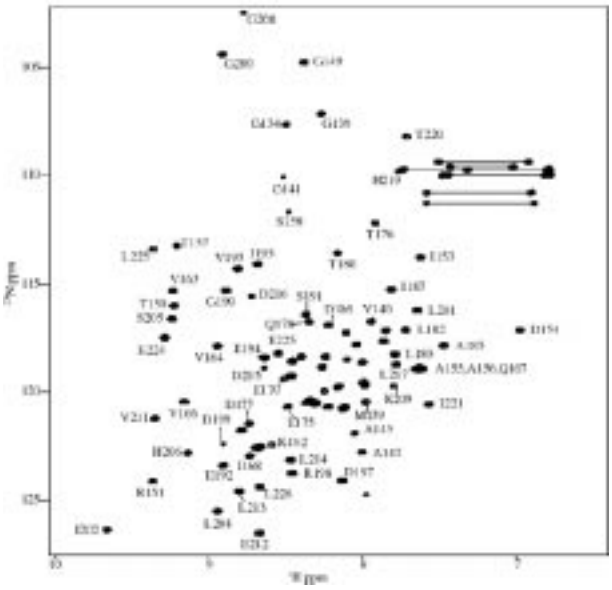

Figure 1: 2D ^{1}H, ^{15}N correlation spectrum of DtxR(130-226), indicating assignments. Some assignments are not indicated for clarity. Correlations due to side chain amides are connected by bars.

Backbone $^{1}H^{N}$, ^{15}N, C^{α}, and C^{β} resonances for individual spin systems were assigned using a combination of 3D HNCACB and CBCA(CO)NH spectra, starting from Ala, Ser, Thr, or Gly residues, which have unique C^{α}/C^{β} chemical shift. The favorable relaxation properties of this domain resulted in complete sets of *i* and *i*-1 correlations in the HNCACB spectrum for nearly all residues, which facilitated complete assignment of the backbone resonances. Backbone carbonyl resonances were assigned from the 3D HNCO spectrum. Aliphatic sidechain proton resonances were assigned from H(C)(CO)NH-TOCSY and HCCH-TOCSY spectra, and further substantiated by analysis of 3D ^{15}N-edited TOCSY-HSQC and NOESY- HSQC spectra. Aromatic resonances were assigned using a combination of heteronuclear and homonuclear (NOESY) 2D experiments. Stereospecific assignments for 33% of the Val and Leu methyl groups were also obtained. Chemical shift index analysis of the backbone assignments indicates the presence of 5 β- strands, and 3 or 4 short helical regions, consistent with the available low resolution crystal structure.